

## Regional Trends in *Nimbus-7* OLR: Effects of a Spectrally Nonuniform Albedo\*

DAVID H. TASHIMA AND DENNIS L. HARTMANN

*Department of Atmospheric Sciences, University of Washington, Seattle, Washington*

(Manuscript received 1 April 1998, in final form 6 July 1998)

### ABSTRACT

Data from the Earth Radiation Budget wide-field-of-view sensors on board the *Nimbus-7* satellite during the period 1979–87 indicate a statistically significant downward trend in daytime outgoing longwave radiation (OLR) of up to  $14 \text{ W m}^{-2} \text{ decade}^{-1}$  over the Sahara desert region of Africa. Reflected solar radiation shows a positive trend of the same magnitude. No significant trends in temperature or cloudiness over the region can be demonstrated. Atmospheric desert dust aerosols increase over the same period, but the spatial pattern of the dust trend is different from that of the OLR and reflected solar trends.

A plausible explanation is that these trends are instrumental in nature and are caused by degradation of the Suprasil filter dome that covers the reflected solar channels. The filter dome degradation is greater for shorter wavelengths of the solar spectrum compared to red and near-infrared wavelengths. This enhanced degradation at shorter wavelengths, combined with the increased albedo of deserts at longer wavelengths, causes the global correction applied to the reflected solar data to be too large over desert regions. The OLR is calculated by subtracting the reflected solar irradiance from the unfiltered total outgoing irradiance (reflected solar plus emitted longwave). Thus, if the total irradiance remains unchanged, an erroneous upward trend in the solar data will cause a downward trend in the OLR estimate of similar magnitude.

A preliminary calculation of the magnitude of the filter degradation effect is presented. Laboratory and thematic mapper spectral reflectance data of desert sand are used to estimate the reflectivity of the desert surface as a function of wavelength. The degradation of the shortwave filter as a function of wavelength is estimated with a quadratic fit to the known deterioration rates of the reflected solar and near-infrared channels. Using these parameters, the magnitude of the trend explained by this effect is calculated to be  $11 \text{ W m}^{-2} \text{ decade}^{-1}$ , which is nearly as large as the trends in the data.

### 1. Introduction

Earth-orbiting satellites provide a useful platform from which to observe variability of the global climate system. To measure variability on timescales of a decade or more requires a highly calibrated instrument, a stable orbit, and precise intercalibration of succeeding instruments contributing to a long-term record. To this point a relatively small number of satellite datasets with the required precision and consistency are available.

The time series of broadband radiation budget measurements taken by the Earth Radiation Budget (ERB) instrument on the *Nimbus-7* satellite provides a relatively consistent set of global radiation budget observations. The instruments began operation in November

1978 and the wide-field-of-view (WFOV) sensors collected data for 15 yr, though only 9 yr have been processed (Kyle et al. 1993a). A wide-field-of-view instrument captures radiation emanating from the entire earth disc, but a large proportion of the captured energy comes from an area with a diameter of about 1000 km centered directly beneath the satellite. The ERB instrument was relatively well calibrated, and for most of its life it remained in a stable sun-synchronous orbit.

Work by Cess (1990) indicates that the globally averaged OLR signal measured by the *Nimbus-7* ERB is highly correlated with an independent measurement of globally averaged surface temperature over the period 1978–87. We set out to look for regional and seasonal structure in this trend.

A number of studies have addressed the problem of removing instrumental biases from the ERB data. Kyle et al. (1995a) address short-term perturbations and Kyle et al. (1995b) examine long-term sensitivity drifts. The corrections applied to the reflected solar data were designed to remove the error from the global mean. While the adjustments to the global mean are quite good, this tactic leaves room for error on the regional scale.

---

\* Joint Institute for the Study of the Atmosphere and Ocean Contribution Number 503.

---

*Corresponding author address:* David Tashima, Department of Atmospheric Sciences, University of Washington, Box 351640, Seattle, WA 98195.  
E-mail: tash@atmos.washington.edu

## 2. Relevant datasets

The primary datasets of interest are the outgoing longwave radiation (OLR) and reflected solar data taken from the *Nimbus-7* ERB instrument. This polar-orbiting satellite crossed the equator near noon and midnight local standard time. Several versions of the data exist; we used the standard collection of datasets, called the ERB MATRIX Summary Tape, or EMST (Kyle et al. 1984; Kyle et al. 1985; Kyle 1990). The data run from November 1978 to October 1987, giving 9 yr of monthly averaged data. Several ERB channels are available, and the data we analyze were derived from the total channel 12 (0.2–50  $\mu\text{m}$ ) and the solar channel 13 (0.2–3.8  $\mu\text{m}$ ). The OLR amount is given by the total channel at night (descending node, or DN) and the difference between total channel and the solar channel during the day (ascending node, or AN). A near-infrared sensor (channel 14) is also available, which is sensitive to frequencies from 0.7 to 2.8  $\mu\text{m}$ .

The in situ station data used to examine surface temperatures were taken from the Global Historical Climatology Network (Vose et al. 1992), which is maintained by the National Climatic Data Center.

To examine cloudiness over the desert, we used the International Satellite Cloud Climatology Project (ISCCP) C2 products (Rossow and Schiffer 1991). The ISCCP data provide global cloud amount information for the period July 1983 to December 1990. The instruments that collected the data use narrowband solar and longwave radiation signals to determine cloudiness variables, which allowed us to corroborate our observations for the overlapping period.

In addition to the ISCCP dataset, in situ cloud data compiled by Hahn et al. (1988) and Hahn et al. (1994) were used to corroborate the satellite data as well as to provide a record of cloudiness that fully covers the time period spanned by the ERB data.

In order to evaluate desert dust aerosols as a potential influence on longwave radiation, we used a dataset derived from radiances taken from the *Nimbus-7* Total Ozone Mapping Spectrometer (TOMS) instrument (Herman et al. 1997). Relative dust quantities were obtained by looking at measured differences between 340- and 380-nm radiances. The dataset covers the globe from 60°N to 60°S and extends from January 1980 until December 1992.

## 3. Analysis

We begin by analyzing the EMST WFOV daytime (ascending node) OLR data taken from the *Nimbus-7* platform. We seek to remove the dominant signals that are well understood and then look for residual variance on interannual timescales. The dominant signal in the OLR is associated with the annual cycle and its harmonics. These can be removed by averaging each month

over the length of the series (9 yr) to obtain an annual climatology, and then subtracting that climatology from the original dataset. Figures 1a–c show the mean, total standard deviation, and the standard deviation of the remaining signal after removing the annual cycle.

The pattern of residual variance appears to be associated with the El Niño–Southern Oscillation (ENSO) phenomenon, as the largest signals reside in the equatorial Pacific. Indeed, when we regress the data against an ENSO index (Niño-3), we find a high coefficient of regression in the equatorial Pacific (Fig. 2). However, not all of the interannual variance associated with ENSO in this region is correlated with the Niño-3 index; there are orthogonal components that are not captured by a single time series.

In order to remove the bulk of the variance associated with ENSO, we apply an empirical orthogonal function (EOF) analysis to the OLR anomalies in the tropical portion of the globe (30°N–30°S). The data is first smoothed with a 3-month running mean in order to eliminate high-frequency (30–60 day) variance associated with the Madden–Julian oscillation (Madden and Julian 1994) that has been aliased into our monthly dataset. The first principal component has a correlation of 0.87 with Niño-3 and exhibits strong peaks for the 1982–83 and 1986–87 events. The actual EOF itself has the characteristic dipole between the east and west Pacific typical of ENSO-like phenomena. Figure 3a is the regression of the first principal component upon the EMST AN OLR data. The second EOF also has a large magnitude in the Pacific (Fig. 3b). These two EOFs are similar to those observed in Bess et al. (1992). Neither of these first two principal components project any significant variance onto regions outside of the tropical oceans, so their removal has little effect upon the trend analysis below. Figure 1d shows the standard deviation of the data after removing both the annual cycle and the first two tropical EOFs.

## 4. Trend analysis

With the annual cycle and ENSO signals removed, we can calculate the trend of the data in order to investigate the regional characteristics of the global trend from Cess (1990). The application of a linear regression against time to the residual OLR after removal of the annual, ENSO, and 30–60-day variance (Fig. 4a) yields two notable features: a large negative trend over the Sahara and Arabian deserts of about 10–15  $\text{W m}^{-2} \text{decade}^{-1}$  and a smaller but more widespread negative trend of about 5  $\text{W m}^{-2} \text{decade}^{-1}$  over most of the landmasses in the mid- and high latitudes of the Northern Hemisphere. We thus find that the global trend of Cess (1990) comes primarily from the Northern Hemisphere land areas. A correlation analysis (Fig. 4b) shows those regions where the trends are statistically different from zero at the 95% confidence level. The correlation sig-

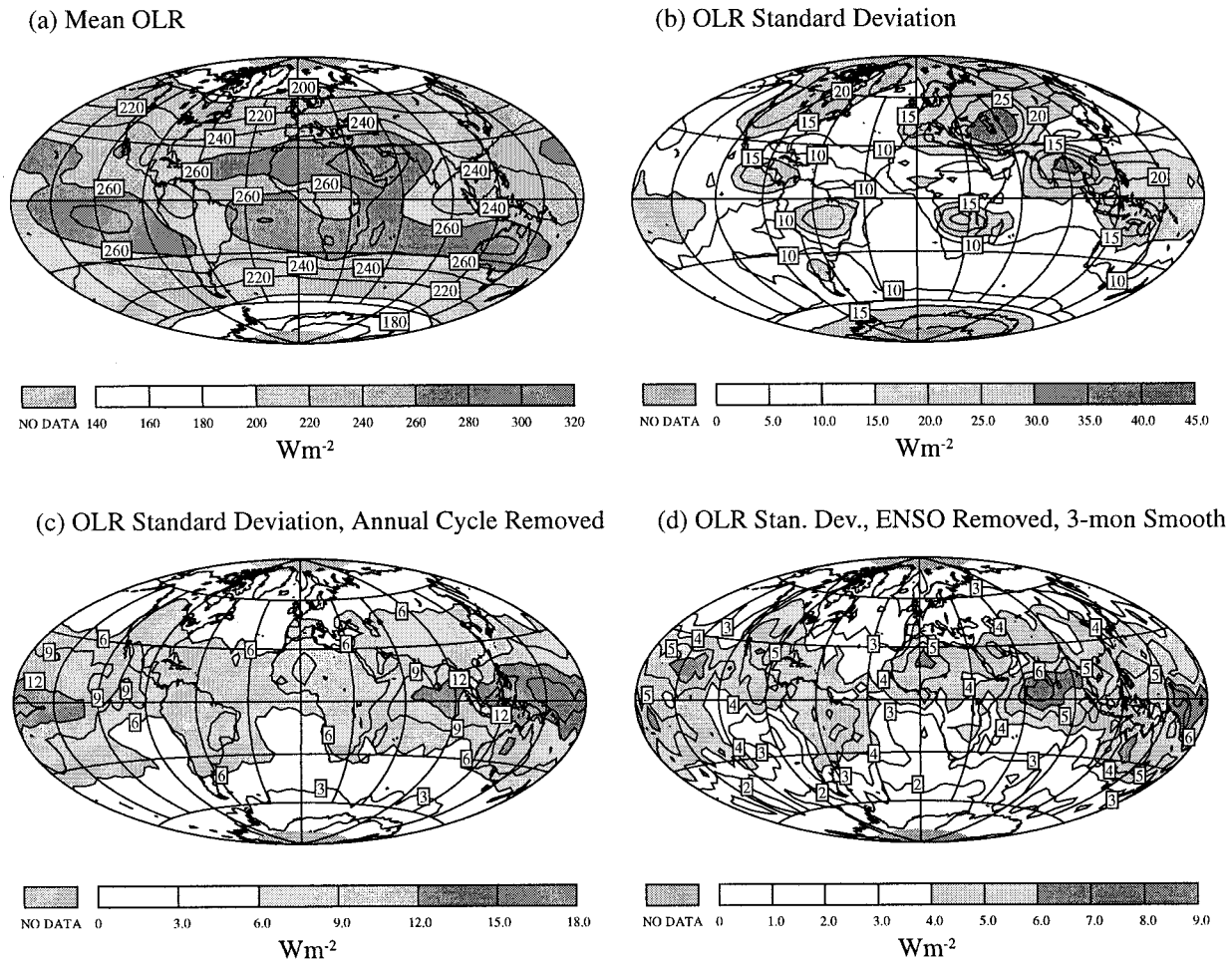


FIG. 1. (a) Mean ERB OLR (EMST, AN), November 1978–October 1987. Contour interval is  $20 \text{ W m}^{-2}$ . Values greater than  $200 \text{ W m}^{-2}$  are shaded, and values greater than  $260 \text{ W m}^{-2}$  are shaded heavily. (b) The standard deviation of monthly ERB OLR (primarily variance associated with the annual cycle). Contour interval is  $5 \text{ W m}^{-2}$ . Values greater than  $15 \text{ W m}^{-2}$  are shaded, and values greater than  $30 \text{ W m}^{-2}$  are shaded heavily. (c) Standard deviation of residual OLR variance after the annual cycle is removed. Most of the variance in the Pacific Ocean is ENSO-related. Contour interval is  $3 \text{ W m}^{-2}$ . Values greater than  $6 \text{ W m}^{-2}$  are shaded, and values greater than  $12 \text{ W m}^{-2}$  are shaded heavily. (d) Same as (c) but smoothed with a 3-month running mean, and the first two ENSO-related EOFs have been removed. Contour interval is  $2 \text{ W m}^{-2}$ . Values greater than  $4 \text{ W m}^{-2}$  are shaded, and values greater than  $6 \text{ W m}^{-2}$  are shaded heavily.

nificance levels we used were found using 21 degrees of freedom, which was estimated from the globally averaged autocorrelation (Leith 1973).

The time series over the Sahara (averaged over the area from  $15^{\circ}$  to  $30^{\circ}\text{N}$ ,  $0^{\circ}$  to  $15^{\circ}\text{E}$ ) shows a steady decline over the entire time period (Fig. 5). The first two EOFs that were removed show little magnitude in this region (the zero line crosses the Sahara in both), and the variance of the OLR anomalies over the Sahara is unchanged by their removal, so we know that the trend is not an artifact of the procedure we used to remove the ENSO signal. The first month (November 1978) should be ignored, as the instrument began taking measurements halfway through the month.

We observe a strong difference in the trend between day and night observations. The EMST dataset can be divided into the daytime, or AN measurements, and

nighttime, or DN measurements. If we perform the same analysis (removing annual cycle and ENSO-related EOF modes, then calculating the trend) on the DN data, we find that the trends over all but a few isolated regions near the poles are negligible.

We also applied the analysis on the reflected solar dataset (removal of the annual cycle and ENSO modes, followed by a trend calculation). The only significant trend is a positive trend over the same region as the OLR trend (the central Sahara desert), with roughly the same magnitude ( $10\text{--}15 \text{ W m}^{-2} \text{ decade}^{-1}$ ). It is possible to imagine OLR trends that only appear at midday and not at midnight, but it seems more likely that instrumental effects may be playing a role. If a trend in the reflected solar data exists and is caused by instrument degradation, it would also show up in the daytime OLR data. It would not show up in the nighttime data, how-

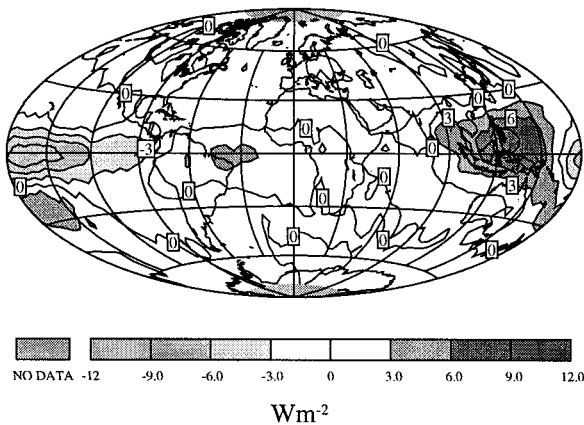


FIG. 2. Regression of the normalized Niño-3 index on EMST AN OLR. Units are  $W m^{-2}$ . Contour interval is  $3 W m^{-2}$ . Values greater than  $6 W m^{-2}$  are lightly shaded, and values less than  $-6 W m^{-2}$  are heavily shaded.

ever, because the nighttime OLR comes from the total channel and requires no differencing.

**5. Exploration of possible physical causes**

Two physical phenomena are generally associated with the reduction of the emitted longwave radiation from a region: a decrease in surface temperature or an increase in the quantity of an infrared absorber in the atmosphere. We will examine both of these possibilities in detail.

A time series of surface temperature anomalies over the region of greatest OLR trend ( $15^{\circ}$ – $30^{\circ}$ N,  $0^{\circ}$ – $15^{\circ}$ E) shows no decreasing trend (Fig. 6). The derivative of emitted blackbody radiative energy with respect to temperature at 300 K is roughly  $6 W m^{-2} K^{-1}$  (from the Stephan–Boltzmann equation), so to produce a trend of  $10$ – $15 W m^{-2} decade^{-1}$ , one would need a trend in

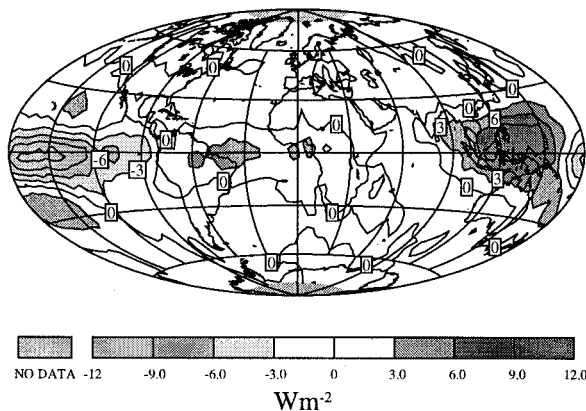
temperature of about  $2 K decade^{-1}$ , which is clearly not observed in the temperature record.

Clouds or water vapor are highly effective infrared absorbers, and an increase in cloudiness over the Sahara region could cause a decrease in OLR. Indeed, an analysis of the ISCCP (satellite) data of cloud frequency over the subject region ( $15^{\circ}$ – $30^{\circ}$ N,  $0^{\circ}$ – $15^{\circ}$ E) indicates a slight increase in cloudiness during the time period overlapped by both datasets: July 1983 to November 1987 (see Fig. 7, bottom series). This trend is confirmed in the set of in situ total cloud amount data (Fig. 7, top series). However, this overlapping time period covers only the latter half of the *Nimbus-7* ERB OLR record. The in situ record, which goes back farther in time, actually shows a decrease in cloudiness for the time period preceding the commencement of the ISCCP measurements. This decrease in cloudiness corresponds with a period of increasing drought in the Sahel.

The final possibility we have investigated is that increasing dust levels are responsible for the trend in OLR. Although dust levels are not measured on a widespread basis, decreases in airport visibility (which is generally only reduced by dust haze) have been observed at many African stations during the period from 1978 to 1986 (N’Tchayi et al. 1994). These visibility reductions occur in conjunction with decreasing precipitation in the Sahel (the region just south of the Sahara that experiences the greatest precipitation variance).

Dust acts to reduce the infrared radiation to space, while simultaneously affecting the amount of reflected solar radiation. The degree to which OLR is reduced by dust depends on the height attained in the atmosphere and the optical thickness of the dust cloud. Dust has been measured to heights of up to 3 km, at optical depths of 1.5 (D’Almeida 1986). Egan (1994) found, using a simple radiative transfer model, that it is possible for a typical dust loading in the atmosphere to reduce top-of-atmosphere OLR by about  $10 W m^{-2}$ , about the order

(a) OLR Regressed on EOF1



(b) OLR Regressed on EOF2

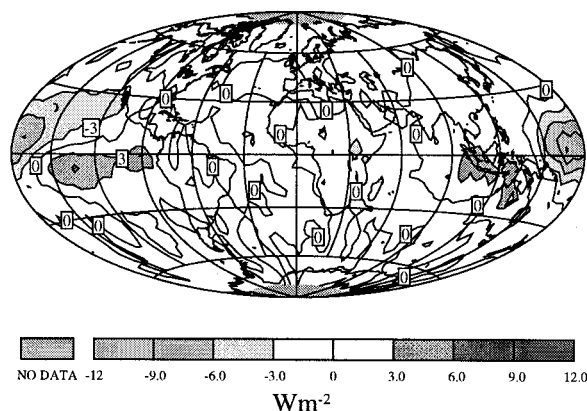


FIG. 3. (a) Regression of the normalized principal component (corresponding to the first EOF of tropical OLR) upon OLR. Units are  $W m^{-2}$ . (b) Same as (a) but using the second principal component.

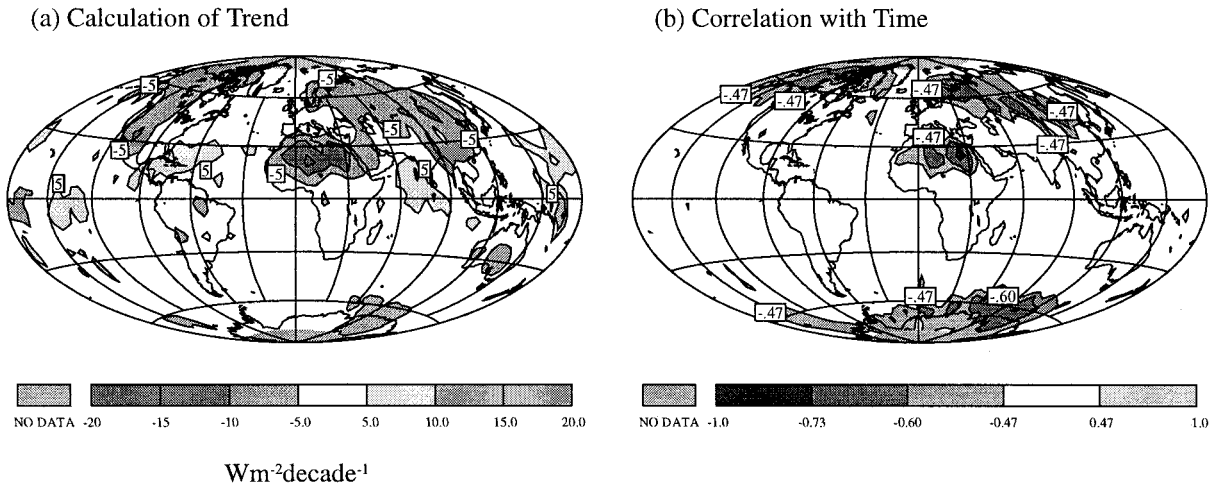


FIG. 4. (a) Calculation of trend (regression with time). Units are  $W m^{-2} decade^{-1}$ . (b) Correlation analysis of trend, using degrees of freedom = 21 (estimated using the global mean autocorrelation). The 0.47 contour represents the areas within which the trend is statistically different from zero at the 95% significance level.

of magnitude of the trend we see over the Sahara. The change in the amount of reflected solar radiation depends on the albedo of the surface below. If the surface is dark, then the dust will increase the reflected solar by a significant amount, whereas a higher albedo surface might be unaffected. In some extreme cases, with a very bright surface, the amount of reflected solar will actually be reduced because the single scattering albedo of dust is less than 1 (Tegen et al. 1996).

Using the *Nimbus-7* TOMS dust aerosol dataset (Herman et al. 1997), we were able to look at relative quantities of dust loading in the atmosphere over most of the ERB record (January 1980–October 1987). Dust levels from this dataset are expressed as a constant times the logarithm of the quotient between the measured backscattered radiance and the radiance calculated from a model. The discrepancy between the two quantities arises in the presence of UV-absorbing aerosols (such as desert dust), which alter the reflective characteristics

as a function of wavelength. The mean  $\Delta N$  residues are shown in Fig. 8a, to present an example of the magnitudes involved. Figure 8b is the calculated trend, after removing the annual cycle and ENSO influences, in  $\Delta N$  per decade. Dustiness shows a strong positive trend, whose magnitude reaches the mean level in some places. The trend shown is statistically significant to the 95% level.

This trend is primarily located on the western edge of North Africa, however, and extends over the tropical Atlantic Ocean as well as over the continent. This does not agree with the spatial pattern of the OLR and reflected solar trends, which are located directly over the middle of the Saharan region. While it might not be unreasonable for the reduction in OLR from dust to be smaller over the ocean than over the desert, it is very unlikely that the increase in reflected solar radiation would be greater over the high albedo desert than over the dark ocean (Carlson and Benjamin 1980). Since re-

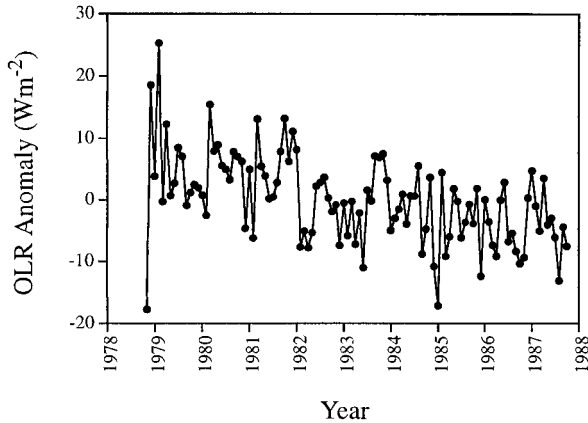


FIG. 5. Time series of EMST AN OLR over Sahara (area defined as  $15^{\circ}$ – $30^{\circ}$ N,  $0^{\circ}$ – $15^{\circ}$ E).

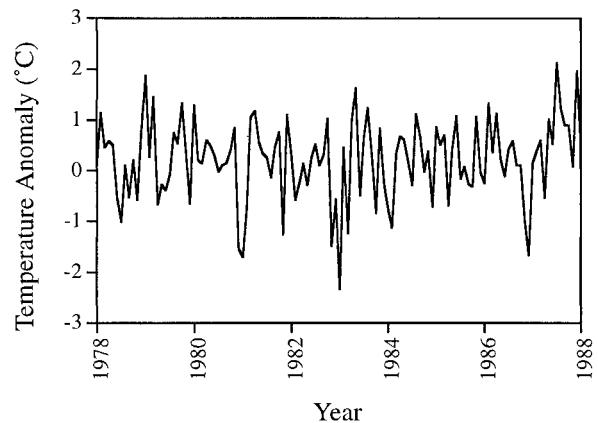


FIG. 6. Time series of temperature anomalies over the Sahara ( $15^{\circ}$ – $30^{\circ}$ N,  $0^{\circ}$ – $15^{\circ}$ E).

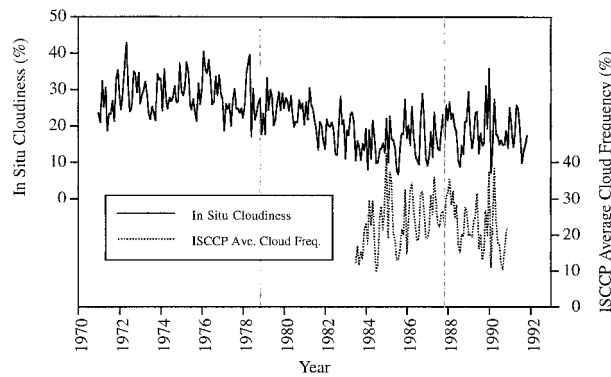


FIG. 7. (top) In situ total cloud cover data from Hahn et al. (1988) and Hahn et al. (1994). (bottom) Time series of ISCCP average cloud amount. Both time series are compiled from data from the region (15°–30°N, 0°–15°E).

flected shortwave does not change significantly over the ocean, we conclude that increases in desert dust quantities are not the explanation for the ERB trend over the desert.

**6. Satellite and instrument effects**

Having considered the reasonable physical causes, we now examine effects caused by properties of the satellite and the instrument. Most polar-orbiting satellites have a precession or drift associated with them. The *Nimbus-7* satellite is no exception, although the drift during the period of operation was very small: roughly half an hour of local time for the 10-yr period. An analysis of the diurnal cycle of OLR over the Sahara by Duvel and Kandel (1985) shows that a change from 1200 LST to 1130 LST yields roughly a 3 W m<sup>-2</sup> difference in OLR. This is significant but too small to explain the magnitude of the trend observed.

The most significant instrumental problem is the degradation of the longwave filter on the shortwave channel

13. Kyle (1990) discusses the declining sensitivity of the reflected shortwave channel over the 10-yr period. A correction for this degradation was applied in the final production of the EMST dataset. The details of the correction can be found in Ardanuy and Rea (1984), Kyle et al. (1984), Kyle et al. (1985), and Kyle et al. (1995b).

Evidence suggests that the clouding of the filter preferentially affects the shorter (or “bluer”) wavelengths of the solar spectrum (Kyle et al. 1995b). The shortwave channel (13) sensitivity decreased 13.2% over the period of the dataset, while the near-infrared channel (14) sensitivity decreased only 6%. Both sensors were covered by the same type of longwave filter, a Suprasil-W dome. Other studies have shown that the deterioration of the transmissivity of these domes increases with decreasing wavelength. The maximum degradation occurs in the ultraviolet portion of the spectrum (Kyle et al. 1993b, appendix B).

The correction that was applied to the ERB shortwave data is independent of wavelength; much of the reflected solar radiation comes from clouds, which have a spectrally flat albedo in the solar wavelengths. If a particular geographical region has a reflectivity spectrum that is not flat but is higher at the long or short wavelengths, then it would be over- or undercorrected, creating an artificial trend.

The desert regions of the earth are unique because they have a relatively high broadband albedo (~0.3), but a very low ultraviolet reflectivity (most of the reflected ultraviolet radiation comes from clouds or snow) (Eck et al. 1987). Laboratory measurements of desert dune sand from Bahariya, Egypt, show that the reflectivity with respect to BaSO<sub>4</sub> decreases significantly with decreasing wavelength (Jacobberger 1989). Thus, the desert surface reflects more radiation in the longer (or “redder”) wavelengths of the solar spectrum. This would lead to an overcorrection of the reflected solar signal.

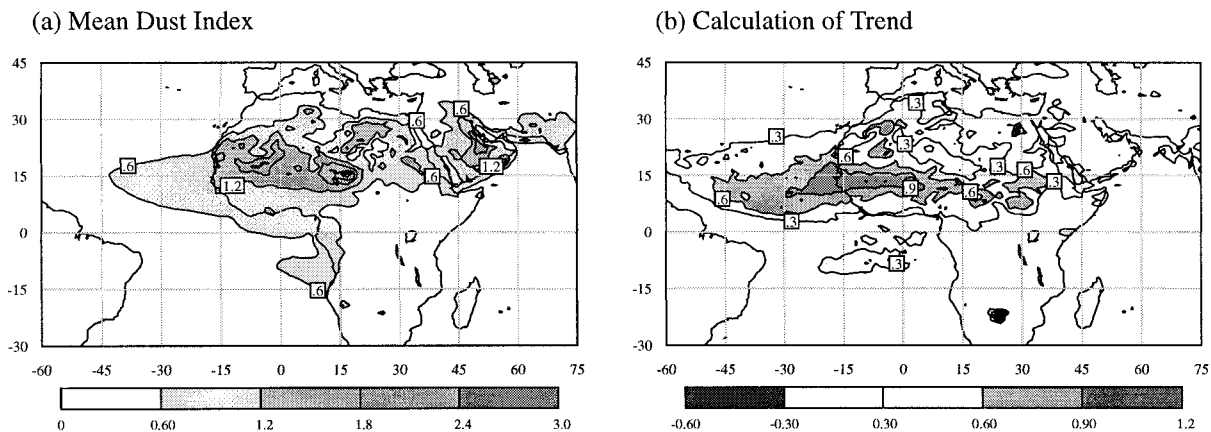


FIG. 8. (a) Mean dust index over North Africa and the tropical Atlantic, calculated using data from the *Nimbus-7* TOMS experiment (1980–87). (b) Calculated trend of dust residues from 1980 to 1987. Units are ΔN decade<sup>-1</sup>.

### 7. Magnitude of the effect of a spectrally asymmetric albedo

We would like to determine if the effect of the interaction between the “red” albedo of the deserts and the “blue” filter deterioration is significant enough to explain the trends observed in the data. To calculate the magnitude of this effect, we must compare the correction that was applied to the data to the correction that takes into account the red albedo of the desert surface. The applied correction is given by

$$C(t) = \frac{F_{\text{real}}}{F_{\text{measured}}} = \frac{\int_{\lambda} F_{\text{sun}}(\lambda)\alpha(\lambda) d\lambda}{\int_{\lambda} D(\lambda, t)F_{\text{sun}}(\lambda)\alpha_0 d\lambda} = \frac{\int_{\lambda} F_{\text{sun}}(\lambda) d\lambda}{\int_{\lambda} D(\lambda, t)F_{\text{sun}}(\lambda) d\lambda}, \quad (1)$$

where  $C(t)$  is the applied correction as a function of time,  $\alpha(\lambda)$  is the albedo of the earth,  $\alpha_0$  is the equivalent wavelength independent albedo,  $F_{\text{sun}}$  is the Planck function, and  $D(\lambda, t)$  is the degradation function (given as the radiation fraction transmitted as a function of wavelength and time).

The correction that is appropriate for the wavelength dependent albedo is

$$C_{\text{desert}}(t) = \frac{F_{\text{real}}}{F_{\text{measured}}} = \frac{\int_{\lambda} F_{\text{sun}}(\lambda)\alpha_{\text{desert}}(\lambda) d\lambda}{\int_{\lambda} D(\lambda, t)F_{\text{sun}}(\lambda)\alpha_{\text{desert}}(\lambda) d\lambda}, \quad (2)$$

where  $\alpha_{\text{desert}}$  is the wavelength-dependent albedo of the desert surface.

The fractional overcorrected error at the end of the time period is simply

$$\text{fractional error} = 1 - \frac{C_{\text{desert}}(t_0)}{C(t_0)}. \quad (3)$$

The resulting trend that would be explained by this effect is then

$$\text{trend explained} = \frac{1}{F_{\text{Sahara}}} (\text{Fractional error}) \frac{10 \text{ yr decade}^{-1}}{9 \text{ yr of data}}, \quad (4)$$

where  $F_{\text{Sahara}}$  is the mean reflected shortwave over the Saharan region (roughly  $280 \text{ W m}^{-2}$ ).

The degradation function at the end of the period,  $D(\lambda, t_0)$ , must be estimated. We know that the reflected solar channel 13 degraded 13.2% and the near-infrared channel 14 degraded 6%. This gives us two pieces of

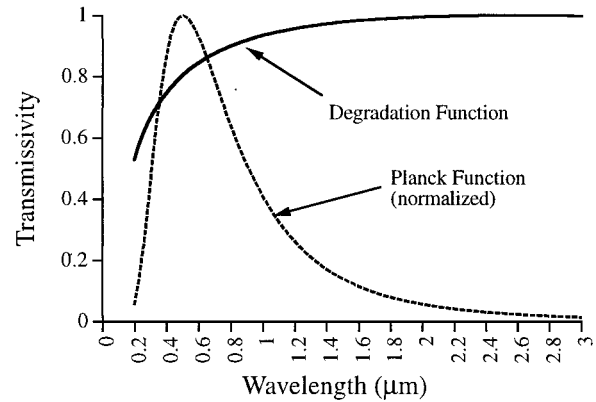


FIG. 9. The degradation function  $D(\lambda, t_0)$ . It is fitted to a quadratic in  $\log(\lambda)$ , with the transmissivity fixed at 1.0 at  $3.0 \mu\text{m}$ .

information with which to fix a function, by integrating the Planck function over the corresponding wavelength range ( $0.2\text{--}3.8 \mu\text{m}$  for the solar channel and  $0.7\text{--}2.8 \mu\text{m}$  for the near-infrared channel).

The simplest choice would be a curve fit that is linear with the natural log of wavelength. This unfortunately results in transmissivities that are much greater than 1.0 for the higher wavelengths. While this would probably have little effect on the result (as the radiative energy at the higher wavelengths represents a small fraction of the total solar energy), it is nonetheless undesirable.

A more suitable choice is to fix a point on the curve and fit the curve to a quadratic of natural log of wavelength. We fixed the transmissivity to be 1.0 at  $3.0 \mu\text{m}$ , which yielded a degradation function given by

$$D(\lambda, t_0) = -[0.07122(\log\lambda)^2] - (1.8308 \log\lambda) - 10.7644. \quad (5)$$

This curve is shown in Fig. 9.

We also need to know the desert reflectance as a function of wavelength. The reflectance data from Jacobberger (1989) was used for the wavelengths between  $0.383$  and  $1.2 \mu\text{m}$ . Some discrepancy exists between the data measured in the laboratory and the thematic mapper (TM) data. While the two sources agree for wavelengths less than  $0.5 \mu\text{m}$ , the TM has slightly lower reflectance values for greater wavelengths, due either to atmospheric effects or the non-Lambertian nature of the surface. In order to represent the most conservative case, the lower reflectance values were used (this acts to reduce the spectral asymmetry of the albedo). Values less than  $0.383 \mu\text{m}$  were set equal to the reflectance at  $0.383 \mu\text{m}$  (again, in order to examine the most conservative case). Values greater than  $1.2 \mu\text{m}$  were set equal to the reflectance at  $1.2 \mu\text{m}$  ( $0.55$ ).

We chose the limits of integration to be from  $0.3$  to  $1.3 \mu\text{m}$ . The lower limit was chosen so as to avoid the effects of ozone absorption in the ultraviolet range. The upper limit was chosen because of the water vapor absorption bands that come into play at wavelengths great-

er than  $1.3 \mu\text{m}$ , which violates the original assumption that the cloud reflectance is uniform with respect to wavelength. This choice also eliminates problems with similar bands of absorption that lie at  $1.4$  and  $1.9 \mu\text{m}$  in the desert surface reflectivity (Leu 1977; P. Buck 1997, personal communication). The near-infrared water vapor absorption bands at wavelengths less than  $1.3 \mu\text{m}$  are small and have little bearing on the result of the integration.

Even though the limits of integration are smaller than the frequency response range of the reflected solar channel, the difference is not too important, for two reasons: 1) the bulk of the energy in the solar spectrum has been accounted for, and 2) the degradation function is relatively shallow for the higher wavelengths (recall that the effect arises from the steepness of both the degradation and the albedo functions).

Using the specifications given above, the fractional error is calculated to be 3.5%, which is equivalent to an absolute trend of  $11 \text{ W m}^{-2} \text{ decade}^{-1}$  (assuming a mean solar reflectance of  $280 \text{ W m}^{-2}$ ). This is in approximate agreement with the trend that is observed in the ERB reflected solar (and OLR) data over the Sahara.

## 8. Conclusions

Our analysis of *Nimbus-7* ERB OLR data reveals a downward trend over the Sahara desert of up to  $14 \text{ W m}^{-2} \text{ decade}^{-1}$ . An upward trend with the same magnitude and spatial pattern is seen in the reflected solar data. The trend in OLR appears only in the daytime data; it is not present in the nighttime data.

In situ temperature measurements from the region show no significant changes in temperature. Cloud frequency data from the ISCCP dataset show an increase in cloudiness (or dustiness) for the second half of the record, but the in situ data of cloud amount reveal that there is no significant trend when the entire record is considered.

Desert dust aerosol levels measured by the *Nimbus-7* TOMS instrument increase over the length of the ERB record but the spatial pattern does not agree with the trend in OLR and reflected shortwave radiation. The trend in dustiness is centered on the west African coast and extends well over the tropical Atlantic Ocean, while the ERB trends are located squarely over the North African continental deserts. If dust were to significantly affect the amount of reflected shortwave radiation, we would expect the increase over the darker ocean to be greater than the increase over the brighter desert surface. Since there is no significant trend over the ocean, we must conclude that dust increases do not explain the radiation trends.

Strong evidence suggests that the deterioration of the filter on the shortwave channel (13) on the *Nimbus-7* ERB was greater in the shorter (or bluer) wavelengths of the solar spectrum. This spectrally asymmetrical clouding and the redder albedo of the Saharan Desert

surface (greater reflection in the longer red and near-infrared wavelengths) combine to produce an overcorrection in the calibration of the shortwave data over desert regions. A preliminary calculation shows that the degree of overcorrection is 3.5%, which explains a trend of roughly  $11 \text{ W m}^{-2} \text{ decade}^{-1}$ .

This calculation by no means presents a full correction for the current calibration. A more complete analysis would use a radiative transfer model to include the appropriate spectral cloud albedo information as well as atmospheric influences. Also, more accurate reflectance data should be used, with special consideration for the non-Lambertian nature of the desert surface (which would add a seasonal aspect to any further correction).

By itself, the trend over North Africa has little bearing on the results of Cess (1990). It contributes only  $-0.13 \text{ W m}^{-2} \text{ decade}^{-1}$  to the globally averaged trend, while the trend calculated by Cess was  $-1.1 \text{ W m}^{-2} \text{ decade}^{-1}$ . At this point, it is not clear whether the "desert effect" plays a significant role in the higher-latitude land areas, where both cloudiness and snow/ice cover become significant factors.

*Acknowledgments.* We would like to thank the following people, whose help made this work possible: Lee Kyle for his advice and suggestions as well as his vast knowledge of the instruments involved; Paul Buck at the Desert Research Institute for additional spectral desert reflectance data; and J. R. Herman and the TOMS Aerosol Group for providing the UV dust index data. This research was funded by the NOAA/NASA cooperative program in Climate Change Data and Detection under NOAA Cooperative Agreement NA67RJ0155. The views expressed herein are those of the authors and do not necessarily reflect the views of NOAA or any of its subagencies.

## REFERENCES

- Ardanuy, P. E., and J. Rea, 1984: Degradation asymmetries and recovery of the *Nimbus-7* ERB shortwave radiometer. *J. Geophys. Res.*, **89** (D4), 5039–5048.
- Bess, T. D., G. L. Smith, T. P. Charlock, and F. G. Rose, 1992: Annual and interannual variations of Earth-emitted radiation based on a 10-year data set. *J. Geophys. Res.*, **97** (D12), 12 825–12 835.
- Carlson, T. N., and S. G. Benjamin, 1980: Radiative heating rates for Saharan dust. *J. Atmos. Sci.*, **37**, 193–213.
- Cess, R. D., 1990: Interpretation of an 8-year record of *Nimbus 7* wide-field-of-view infrared measurements. *J. Geophys. Res.*, **95**, 16 653–16 657.
- D'Almeida, G. A., 1986: A model for Saharan dust transport. *J. Climate Appl. Meteor.*, **25**, 903–916.
- Duvel, J. P., and R. S. Kandel, 1985: Regional-scale diurnal variations of outgoing infrared radiation observed by METEOSAT. *J. Climate Appl. Meteor.*, **24**, 335–349.
- Eck, T. F., P. K. Bhartia, P. H. Hwang, and L. L. Stowe, 1987: Reflectivity of Earth's surface and clouds in ultraviolet from satellite observations. *J. Geophys. Res.*, **92**, 4287–4296.
- Egan, W. G., 1994: Radiative transfer properties of the Sahara region. *Remote Sens. Environ.*, **50**, 182–193.
- Hahn, C. J., S. G. Warren, J. London, R. L. Jenne, and R. M. Chervin,

- 1988: Climatological data for clouds over the globe from surface observations. Rep. NDP-026, Carbon Dioxide Information Analysis Center, Oak Ridge National Laboratory, Oak Ridge, TN, 54 pp. [Available from Carbon Dioxide Information Analysis Center, Oak Ridge National Laboratory, Oak Ridge, TN 37831-6335.]
- , —, and —, 1994: Climatological data for clouds over the globe from surface observations, 1982–1991: The Total Cloud Edition. Rep. NDP-026A, Carbon Dioxide Information Analysis Center, Oak Ridge National Laboratory, Oak Ridge, TN, 42 pp. [Available from Carbon Dioxide Information Analysis Center, Oak Ridge National Laboratory, Oak Ridge, TN 37831-6335.]
- Herman, J. R., P. K. Bhartia, O. Torres, C. Hsu, C. Seftor, and E. Celarier, 1997: Global distributions of UV-absorbing aerosols from Nimbus-7/TOMS data. *J. Geophys. Res.*, **102**, 16 911–16 922.
- Jacobberger, P. A., 1989: Reflectance characteristics and surface processes in stabilized dune environments. *Remote Sens. Environ.*, **28**, 287–295.
- Kyle, H. L., 1990: The Nimbus-7 Earth Radiation Budget (ERB) data set and its uses. Long-Term Monitoring of the Earth's Radiation Budget. *Proc. SPIE*, **1299**, 27–39.
- , F. B. House, P. E. Ardanuy, H. Jacobowitz, R. H. Maschhoff, and J. R. Hickey, 1984: New in-flight calibration adjustment of the NIMBUS 6 and 7 Earth Radiation Budget wide field of view radiometers. *J. Geophys. Res.*, **89**, 5057–5076.
- , P. E. Ardanuy, and E. J. Hurley, 1985: The status of the Nimbus-7 ERB earth radiation budget data set. *Bull. Amer. Meteor. Soc.*, **66**, 1378–1388.
- , and Coauthors, 1993a: The Nimbus Earth Radiation Budget (ERB) Experiment: 1975 to 1992. *Bull. Amer. Meteor. Soc.*, **74**, 815–830.
- , D. V. Hoyt, B. J. Vallette, J. R. Hickey, and R. H. Maschhoff, 1993b: Nimbus-7 Earth Radiation Budget calibration history—Part I: The solar channels. NASA RP 1316, 82 pp.
- , R. Hucek, P. Ardanuy, J. Hickey, R. Maschhoff, L. Penn, and B. Groveman, 1995a: In-flight calibration of the Nimbus-7 Earth Radiation Budget (ERB) sensors. Part II: Short-term perturbations. *J. Atmos. Oceanic Technol.*, **12**, 1150–1162.
- , —, —, L. Penn, and B. Groveman, 1995b: In-flight calibration of the Nimbus-7 Earth Radiation Budget (ERB) sensors. Part III: Long-term changes. *J. Atmos. Oceanic Technol.*, **12**, 1163–1176.
- Leith, C. E., 1973: The standard error of time-averaged estimates of climatic means. *J. Appl. Meteor.*, **12**, 1066–1069.
- Leu, D. J., 1977: Visible and near-infrared reflectance of beach sands: A study on the spectral reflectance/grain size relationship. *Remote Sens. Environ.*, **6**, 169–182.
- Madden, R. A., and P. R. Julian, 1994: Observations of the 40–50-day tropical oscillation—A review. *Mon. Wea. Rev.*, **122**, 814–837.
- N'Tchayi, G. M., J. Bertrand, M. Legrand, and J. Baudet, 1994: Temporal and spatial variations of the atmospheric dust loading throughout West Africa over the last thirty years. *Ann. Geophys.*, **12**, 265–273.
- Rossow, W. B., and R. A. Schiffer, 1991: ISCCP cloud data products. *Bull. Amer. Meteor. Soc.*, **72**, 2–20.
- Tegen, I., A. A. Lacis, and I. Fung, 1996: The influence on climate forcing of mineral aerosols from disturbed soils. *Nature*, **380**, 419–422.
- Vose, R. S., R. L. Schmoyer, P. M. Steurer, T. C. Peterson, R. Heim, T. R. Karl, and J. K. Eischeid, 1992: The Global Historical Climatology Network: Long-term monthly temperature, precipitation, sea level pressure, and station pressure data. Rep. ORNL/CDIAC-53, NDP-041, Carbon Dioxide Analysis Center. [Available from the Carbon Dioxide Information Analysis Center, Oak Ridge National Laboratory, Oak Ridge, TN 37831-6335; or online at <http://cdiac.esd.ornl.gov/epubs/ndp/ndp041/ndp041.html>.]